Journal of Materials Chemistry A

RSC Publishing

PAPER

View Article Online
View Journal | View Issue

Cite this: J. Mater. Chem. A, 2013, 1, 7913

Improved performance of electric double layer capacitor using redox additive (VO^{2+}/VO_2^+) aqueous electrolyte†

S. T. Senthilkumar,[a] R. Kalai Selvan,*[a] N. Ponpandian,[b] J. S. Melo[c] and Y. S. Lee[d]

Received 9th March 2013
Accepted 22nd April 2013

DOI: 10.1039/c3ta10998d

www.rsc.org/MaterialsA

Electric double layer capacitors (EDLCs) were fabricated using biomass derived porous activated carbon as electrode material with 1 M H_2SO_4 and $VOSO_4$ added 1 M H_2SO_4 as electrolytes. Here, $VOSO_4$ was used as redox additive to improve the overall performance of EDLC. As expected, the $VOSO_4$ electrolyte showed ~43% of improved specific capacitance of 630.6 F g^{-1} at 1 mA cm^{-2} compared to pristine 1 M H_2SO_4 (440.6 F g^{-1}) due to the contribution of VO^{2+}/VO_2^+ redox reaction at the electrode–electrolyte interface. Possible redox reaction mechanism of VO^{2+}/VO_2^+ pair is also briefly illustrated. The good cycling performance of 97.57% capacitance retention was observed even after 4000 cycles. For comparison, the polymer gel electrolyte ($PVA/VOSO_4/H_2SO_4$) was also prepared and then the performance of the fabricated EDLCs was studied. Overall, these findings could open up a simple and cost effective way to improve the performance of EDLCs significantly.

1 Introduction

In recent times the electric double layer capacitors (EDLCs) have been identified as one of the foremost energy storage devices due to their versatile properties like good safety, fast charging–discharging, long cycle life and higher power density than batteries.[1,2] However, the EDLCs (*i.e.*, carbon based materials as electrode materials) have delivered the nominal specific capacitance (~150 F g^{-1}) and energy density (4–5 W h kg^{-1}) in liquid electrolytes (*i.e.*, aqueous and alkali) due to their limiting factor of low water decomposition potential of 1.23 V.[3] In order to enhance the performance of EDLCs generally two different methods have been adopted in the carbon based materials. In one, heteroatoms such as oxygen,[4] nitrogen,[4] phosphorous[5] and boron[6] are introduced into the carbon materials and in the second, composites are made with carbon materials like carbon-metal oxide ($Ni(OH)_2$/MWCNT, MgO/CNT and MnO_2/graphene)[7a–c] and carbon-conducting polymer (PANI/carbon sphere, PANI/graphene, PANI/carbon nanocoil, PPY/carbon nanocoil and PPY/GO).[8a–d] However, both the methods have their own disadvantages including declining carbon conductivity, poor cycle stability and multi-step process of composite preparation. In order to overcome these difficulties, very recently an innovative approach of adding redox species into the electrolytes (*i.e.*, redox electrolyte) was introduced to improve the performance of EDLCs *via* electron transfer at electrode–electrolyte interface through reversible redox reactions. This technique is very simple and cost effective approach compared with composite preparation. Organic compounds are mostly used as redox-active compounds due to their better solubility on electrode surface during redox process. Notably, the hydroquinone redox-active electrolyte delivered the maximum specific capacitance of 901 F g^{-1} unfortunately this system retained 65% of its initial specific capacitance after 4000 cycles. Similarly, indigo carmine,[2] methylene blue[9] and sodium lignosulfonate,[10] *p*-phenylenediamine[11,12] and *m*-phenylenediamine[13] have also been reported as redox-active compounds but these have not reached the specific capacitance of hydroquinone redox-active electrolyte (901 F g^{-1}). Thus the impetus is to find new or alternative redox additives to improve the specific capacitance with better cycle performance.

Here we present an alternative approach of using inorganic compound, $VOSO_4$ as a source of VO^{2+} *i.e.*, redox additive in H_2SO_4 electrolyte. It is well known that VO^{2+}/VO_2^+ is one of the most important ionic species in vanadium redox flow batteries because it exhibits the reversible redox reaction at electrode–electrolyte interface and improves their energy storage performance.[14a] Also, their abundance, economical and excellent solubility in aqueous medium favors its use. But, the VO^{2+}/VO_2^+ redox reaction has slower kinetics compared to V^{3+}/V^{2+}.[14b] However, the redox reaction of VO^{2+}/VO_2^+ is enhanced through catalytic process using hydroxyl or carbonyl functionalized carbon materials[14a,c] and carbon supported $CuPt_3$ (ref. 14b) as electrodes resulting in a better improved VO^{2+}/VO_2^+ redox reaction in

[a]Solid State Ionics and Energy Devices Laboratory, Department of Physics, Bharathiar University, Coimbatore-641 046, India. E-mail: selvankram@buc.edu.in; Fax: +91 422 2425706; Tel: +91 422 2428446

[b]Department of Nanoscience and Technology, Bharathiar University, Coimbatore-641 046, India

[c]Nuclear Agriculture and Biotechnology Division, BARC, Trombay, Mumbai-400 085, India

[d]Faculty of Applied Chemical Engineering, Chonnam National University, Gwangju 500-757, Korea

† Electronic supplementary information (ESI) available: See DOI: 10.1039/c3ta10998d

vanadium redox flow batteries. In this connection, here we tried to enhance the performance of the bio-waste derived activated carbon used EDLC using $VOSO_4$ added electrolyte through their VO^{2+}/VO_2^+ redox reaction. Also, here it is found that the $VOSO_4$ added 1 M H_2SO_4 electrolyte showed ~43% of improved specific capacitance of 630.6 F g^{-1} at 1 mA cm^{-2} compared to pristine 1 M H_2SO_4 (440.6 F g^{-1}) and good cycling performance (97.57% retention) was also obtained for 4000 cycles.

2 Experimental section

The activated carbons (ACs) were prepared from *Eichhornia crassipes* by chemical activation using NaOH as reported by us earlier.[15] Briefly, the dried pieces of *Eichhornia crassipes* were pulverized. Then, 20 g of pre-heated (at 200 °C for overnight) pulverized sample was activated in 10% of NaOH for 24 h. Subsequently, it was carbonized at different temperatures such as 600 °C (NaA-1), 700 °C (NaA-2) and 800 °C (NaA-3) for 2 h under Ar atmosphere. The carbonized samples were washed several times with distilled H_2O with desired amount of HCl until the pH reached neutral. The washed samples were dried at 100 °C for overnight.

The prepared ACs was studied by powder XRD using X'Pert PRO PANalytical X-ray Diffractometer. The surface area, pore size and pore distribution of the ACs were carried out using nitrogen adsorption–desorption experiments at 77 K (Micromeritics ASAP 2010 surface area analyser) and calculated by BET method and BJH method, respectively. FTIR spectra of the ACs were recorded with model, Bruker tensor 27. The X-ray photoelectron spectroscope (XPS) was also examined for AC using a Perkin-Elmer PHI-5702. The microscopic porous structure of the AC was observed *via* scanning electron microscopy (SEM) (Quanta 200 ESEM, FEI, USA).

The electrodes for EDLCs were prepared by drop-caste method.[16a] Initially, the slurry was prepared by mixing of AC (20 mg), carbon black (2 mg) and polyvinylidene fluoride (PVDF, 2 mg) in 0.4 mL of *N*-methyl-2-pyrrolidone (NMP). Further, 12 μL of this slurry was spread onto the stainless steel with an area of 1 cm^2 and dried at 50 °C for overnight. The active material loading was calculated to be 0.6 mg on each electrode (excluding carbon black and PVDF mass). Finally, EDLCs (1 M H_2SO_4 and $VOSO_4$ added 1 M H_2SO_4) were fabricated by electrode sandwich type where electrolyte (1 M H_2SO_4 or 0.3 g $VOSO_4$ added 1 M H_2SO_4) immersed polypropylene sheet was used as separator, individually.

To optimize the electrode, electrochemical properties of the AC electrodes were studied by cyclic voltammetry (CV) and galvanostatic charge–discharge (GCD) in 1 M H_2SO_4 using three electrode systems (AC-working electrode, Pt wire-counter electrode and Ag/AgCl-reference electrode). Subsequently, fabricated EDLCs were examined through CV, GCD, electrochemical impedance spectroscopy (EIS) and cycle life. Here, CV and GCD tests for EDLCs were performed in the potential range of 0 to 0.8 V at various scan rates (5–200 mV s^{-1}) and current densities from 1 to 20 mA cm^{-2}, respectively. Electrochemical impedance spectroscopy (EIS) measurements were accomplished by applying an AC voltage with 10 mV amplitude in the frequency range from 100 mHz to 1 MHz at open circuit voltage (OCV). All the electrochemical studies were carried out with Bio-Logic SP150 at room temperature. Besides, the EC-Lab V10.12 software was used for fitting the EIS data.

The specific capacitance of cell (C_{cell}) and specific capacitance of single electrode (C_{SP}) was calculated using the following eqn,[17a]

$$C_{cell} = \frac{I\Delta t}{M\Delta V} \text{ and } C_{SP} = 4C_{cell} \quad (1)$$

where, I is the applied current, M is the total mass of the active material (AC) in both electrodes, Δt is the discharge time, ΔV is the potential range after IR drop.

Similarly, the energy and power density and coulombic efficiency was calculated using the following eqn,[17a,16b]

$$E_{cell} = \frac{C_{cell}\Delta V^2}{7.2}; P_{cell} = \frac{E_{cell}}{\Delta t} \text{ and } \eta = \frac{\Delta t_d}{\Delta t_c} \quad (2)$$

where, Δt_d is the discharging time and Δt_c is the charging time.

The average discharge current (I_d) from cyclic voltammogram, areal capacitance (C_a) and mean areal capacitance (C_m) were obtained using the following eqn,[17a–c]

$$I_d = \frac{\int I dv}{2\Delta V}; \; C_a = \frac{I_d}{sA} \text{ and } C_m = \frac{\Delta I}{2\Delta s} \quad (3)$$

where, $\int I dv$ is the integral area of CV curve, ΔV is the voltage difference, s is the scan rate, A is the area of active material in electrolyte and $\frac{\Delta I}{\Delta s}$ is the slope value.

3 Results and discussion

Fig. 1 shows, the nitrogen (N_2) adsorption–desorption isotherm, pore size distribution and the relation between the pore size

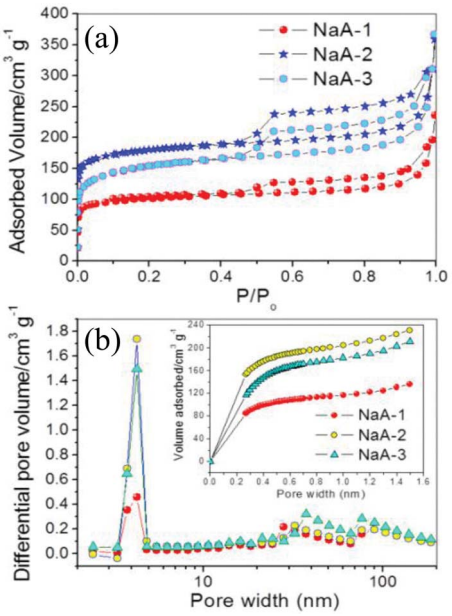

Fig. 1 (a) N_2 adsorption–desorption isotherm; (b) pore size distribution and pore width *vs.* volume adsorbed (inset) of NaA-1, NaA-2 and NaA-3.

and adsorbed pore volume of the prepared ACs at different temperatures such as 600 °C (NaA-1), 700 °C (NaA-2) and 800 °C (NaA-3). All the ACs show (Fig. 1a) the hysteresis loop at above $P/P_0 = 0.4$ between the adsorption–desorption branch which describes that the prepared ACs are mesoporous (2–50 nm) materials. The observed small tail at above $P/P_0 = 0.9$ indicates the presence of macropores (>50 nm). Also, at below $P/P_0 = 0.4$ is because of existence of micropores.[19] The peaks centered at 4.3 nm, ~33 nm and ~82 nm (Fig. 1b) infers the presence of a combination of mesopores and macropores. Among the ACs, NaA-2 exhibits the highest BET surface area of 683.26 $m^2\ g^{-1}$ compared to NaA-1 (381.64 $m^2\ g^{-1}$) and NaA-3 (559.11 $m^2\ g^{-1}$). Moreover among the ACs, NaA-2 shows a larger saturated adsorbed volume (Fig. 1b (inset)) which indicates a higher surface area.[18–20]

The representative SEM, XRD and XPS images of NaA-2 are shown in Fig. 2. Fig. 2a illustrates the SEM image of AC which indicates the porous morphology and it is an evidence for the fact that AC has an interconnected porous structure. From XRD pattern (Fig. 2b), a strong carbon peak is observed in between 20° and 30° which corresponds to the (002) plane and indicates that the AC contains small disordered structure of aromatic sheets or disordered carbon. The other broad peak around 43° is attributed to the plane of (001) diffraction and indicates the presence of sp^2 hybridized carbon of aromatic structure.[21] The FT-IR spectrum (Fig. S1†) shows the characteristic peak at ~3400 cm^{-1} which corresponds to O–H stretching vibrations of hydroxyl group in phenol or carboxylic acid or adsorbed water. The broad peak at 2900–2100 cm^{-1} is due to –C–H stretching. Similarly, the band at 1300–1030 cm^{-1} is ascribed to –C–O stretching vibrations of hydroxyl or ether and O–H bending vibrations. The observed peaks at 1563 cm^{-1} are attributed to stretching vibrations of carbonyl groups (C═O).[22,23] In addition, the presence of surface functional groups was examined by XPS and its representative C 1s and O 1s core level spectra of NaA-2 are shown in Fig. 2c and d. The obtained convoluted three peaks at 284.4 eV, 285.4 eV and 287.3 eV correspond to C 1s spectra and is attributed to presence of graphitic (C–C) or C–H groups, hydroxyl groups C–OH or and carbonyl/quinone groups (C═O). The O 1s core level spectra contains the four peaks such as 531.6 eV, 533.2 eV, 534.6 eV and 535.8 eV ascribed to the carbonyl/quinone groups (C═O), hydroxyl groups (C–OH) in phenol, hydroxyl groups in carboxylic (O═C–OH) acid and chemisorbed water, respectively.[22,23] From the spectral analysis it can be concluded that the hydroxyl functional groups are mostly presented on NaA-2 sample.

In order to optimize the electrode, the CV and GCD tests are carried out for all the samples using a three electrodes system. The obtained CV curves (5 mV s^{-1}) and charge–discharge curves (1 mA cm^{-2}) of AC electrodes (NaA-1, NaA-2 and NaA-3) are shown in Fig. 3. The quasi-rectangular CV curves are obtained for all the ACs, which is the characteristic feature of pseudo-capacitance. This behaviour is due to the reversible redox reaction between the oxygen functionalities like carbonyl (C═O), hydroxyl (C–OH, O–C═O) and H^+.[24,25] The presence of these kind of functional groups are identified through FT-IR and XPS analysis. Nonetheless, the NaA-2 electrode covers a larger current area in CV than NaA-1 and NaA-3 which reveals a higher ionic storage capacity which in turn reflects a higher capacitance. Similarly, the maximum specific capacitance of 587 F g^{-1} was calculated from charge–discharge curve at 1 mA cm^{-2} for NaA-2 while it is 528 F g^{-1} and 420 F g^{-1} for NaA-1 and NaA-3 respectively. This higher specific capacitance may be due to the high surface area of NaA-2 (683.26 $m^2\ g^{-1}$). Overall, NaA-2 is deemed a better and optimal AC electrode for EDLC fabrication.

In order to identify the effect of $VOSO_4$ concentration in 1 M H_2SO_4, the cyclic voltammogram (CV) and electrochemical impedance spectroscopy (EIS) were carried out. The CV curves of NaA-2 electrode in different amounts of $VOSO_4$ (0.2 g, 0.3 g, 0.4 g and 0.5 g) added 1 M H_2SO_4 electrolyte is shown in Fig. 4a, which shows the quasi-rectangular behaviour. Fig. 4b shows the calculated discharge current behaviour of various content of $VOSO_4$ at different scan rates. The calculated areal capacitance are 134 mF cm^{-2}, 188 mF cm^{-2}, 164 mF cm^{-2} and 172 mF cm^{-2} at lower scan rate of 5 mV s^{-1} and 384 mF cm^{-2}, 458 mF cm^{-2}, 369 mF cm^{-2} and 377 mF cm^{-2} at higher scan rate of 50 mV s^{-1} for 0.2 g, 0.3 g, 0.4 g and 0.5 g of $VOSO_4$ respectively. However, the maximum areal capacitance at both lower and higher scan

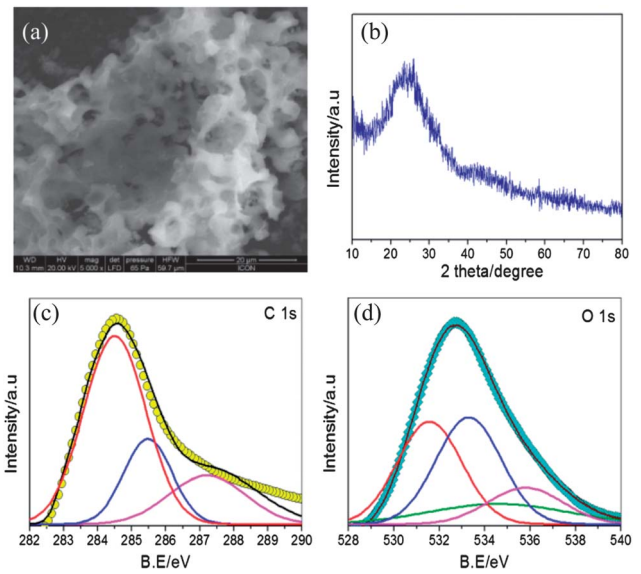

Fig. 2 The typical (a) SEM image; (b) XRD pattern; (c and d) C 1s and O 1s core level spectra of NaA-2.

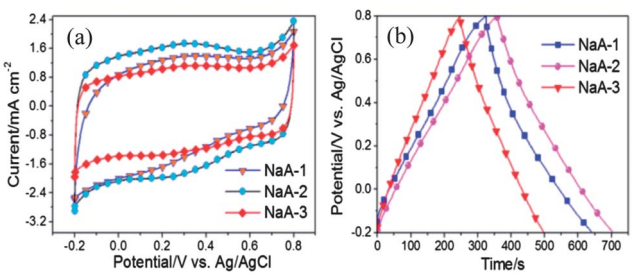

Fig. 3 Electrochemical characterization of AC (NaA-1, NaA-2 and NaA-3) electrodes: (a) CV curves at 5 mV s^{-1}; (b) charge–discharge curves at 1 mA cm^{-2}.

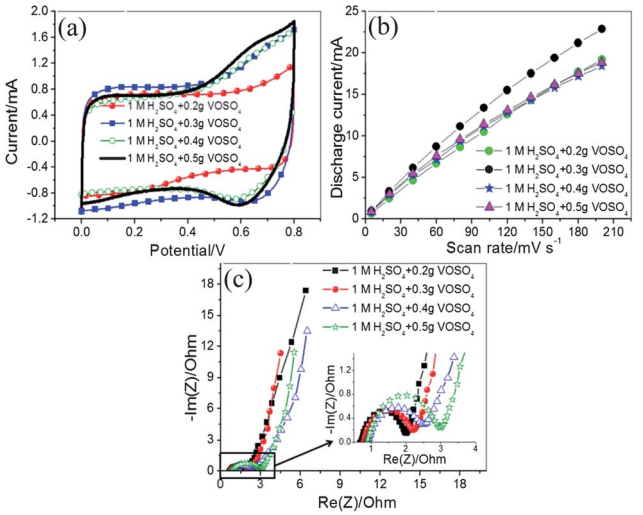

Fig. 4 (a) CV curves of NaA-2 electrode in different amount of $VOSO_4$ added 1 M H_2SO_4 electrolyte; (b) discharge current as function of scan rate; (c) Nyquist plot of $VOSO_4$ added 1 M H_2SO_4 electrolyte at different amount of $VOSO_4$.

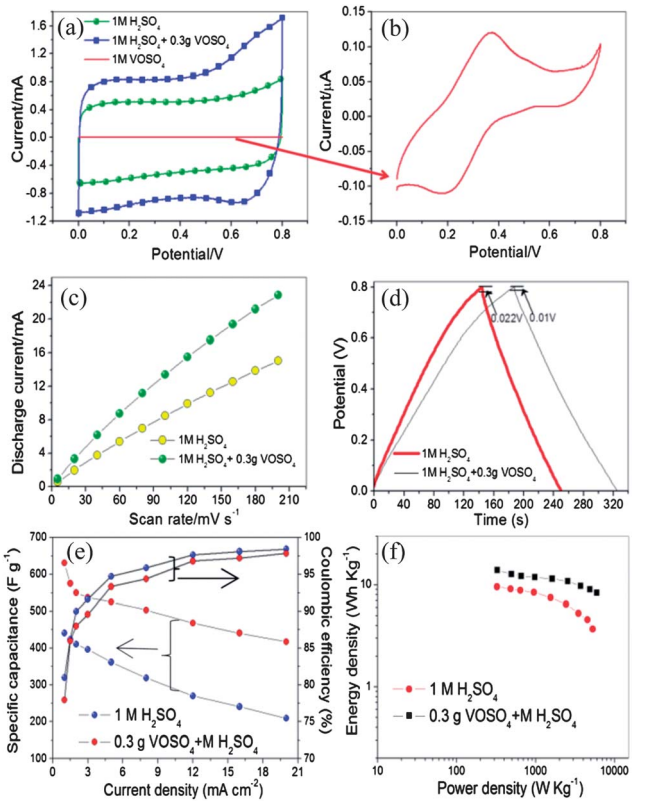

Fig. 5 Electrochemical characteristics of liquid electrolyte using EDLC: (a) comparison of CV curves of 1 M $VOSO_4$, 1 M H_2SO_4 and $VOSO_4$ + 1 M H_2SO_4 electrolyte at 5 mV s^{-1}; (b) CV curve of 1 M $VOSO_4$ electrolyte for clarity; (c) scan rate as a function of discharge current; (d) comparison of charge–discharge curves of 1 M H_2SO_4 and $VOSO_4$ + 1 M H_2SO_4 electrolyte at 1 mA cm^{-2}; (e) specific capacitance and coulombic efficiency as a function of current rate and (f) Ragone plot.

rate as well as better linear discharge current behavior was noted for 0.3 g of $VOSO_4$, which indicates its better electrochemical properties. Moreover, the observed semicircle in Nyquist plot (Fig. 4c) is shifted along the impedance real axis as well as diameter of the semicircle is increased with increasing amount of $VOSO_4$. This reveals the increased charge transfer resistance. However, due to the better discharge current behavior of 0.3 g $VOSO_4$ added H_2SO_4 electrolyte, it is considered as optimal concentration for EDLC and further studied as follows.

Fig. 5a shows the cyclic voltammogram of EDLCs using 1 M H_2SO_4, 1 M H_2SO_4 + 0.3 g $VOSO_4$ and 1 M $VOSO_4$ as electrolyte at 5 mV s^{-1}. The rectangular-like shape CV curve observed for 1 M H_2SO_4 electrolyte, infers electric double layer capacitance and its interfacial capacitance was 90 mF cm^{-2}. Interestingly quasi-rectangular shaped CV curve with increased interfacial capacitance of 150 mF cm^{-2} was observed for $VOSO_4$ (0.3 g) added electrolyte. This quasi-rectangular behaviour is due to the redox reaction of VO^{2+}/VO_2^+. This was further confirmed through the CV (Fig. 5b) of EDLC using 1 M $VOSO_4$ as electrolyte, where it clearly indicates the well defined redox peak. Fig. 5c shows the discharge current response of EDLC using 1 M H_2SO_4 and $VOSO_4$ added 1 M H_2SO_4 as electrolyte with respect to scan rate. As expected higher discharge current was observed for the $VOSO_4$ with EDLC, which is due to the occurrence of redox reaction between VO^{2+}/VO_2^+. From Fig. 5c, the maximum mean areal capacitance of 55.8 mF cm^{-2} was calculated for $VOSO_4$ added 1 M H_2SO_4 electrolyte but it is only 37 mF cm^{-2} for 1 M H_2SO_4 electrolyte. So the combination of $VOSO_4$ (0.3 g) and 1 M H_2SO_4 could improve the performance of pristine electrolyte (1 M H_2SO_4) used EDLC through the possible redox reaction of VO^{2+}/VO_2^+ at electrode–electrolyte interface. The possible redox reaction is given below.

$$VO^{2+} + H_2O \leftrightarrow VO_2^+ + 2H^+ + e^- \quad (4)$$

Furthermore, the redox reaction of VO^{2+}/VO_2^+ is enhanced by catalytic reaction in presence of hydroxyl (–OH) and carbonyl (C═O) functional groups *via* oxygen transfer (Scheme 1). More specifically, during charging in the case of hydroxyl groups (Scheme a), the adsorbed VO^{2+} on the electrode replaces the H^+ from hydroxyl group and creates the bond. Then, the oxygen atom is transferred and forms VO_2^+ on the surface of electrode by releasing of H^+ and e^-. Finally, the VO_2^+ diffuses into the bulk solution *via* exchange of H^+ from bulk solution. In contrast, in the case of carbonyl groups (Scheme b) the adsorbed VO^{2+} creates the transition state with carbonyl groups. Subsequently, it reacts with H_2O while the VO_2^+ diffuses back into the bulk electrolyte as VO_2^+ through release of H^+ and e^-.[26,27a] In addition, during discharge these reactions are reverse of the charging process. So, the hydroxyl and carbonyl functional groups also help the redox reaction of VO^{2+}/VO_2^+ *via* catalytic process.

The galvanostatic charge–discharge curves of EDLCs at 1 mA cm^{-2} are shown in Fig. 5d. The calculated specific capacitances from GCD are 440.6 and 630.6 F g^{-1}. Here, the 1 M H_2SO_4 + $VOSO_4$ electrolyte exhibits the higher specific capacitance with ~43% of improved specific capacitance than pristine 1 M H_2SO_4

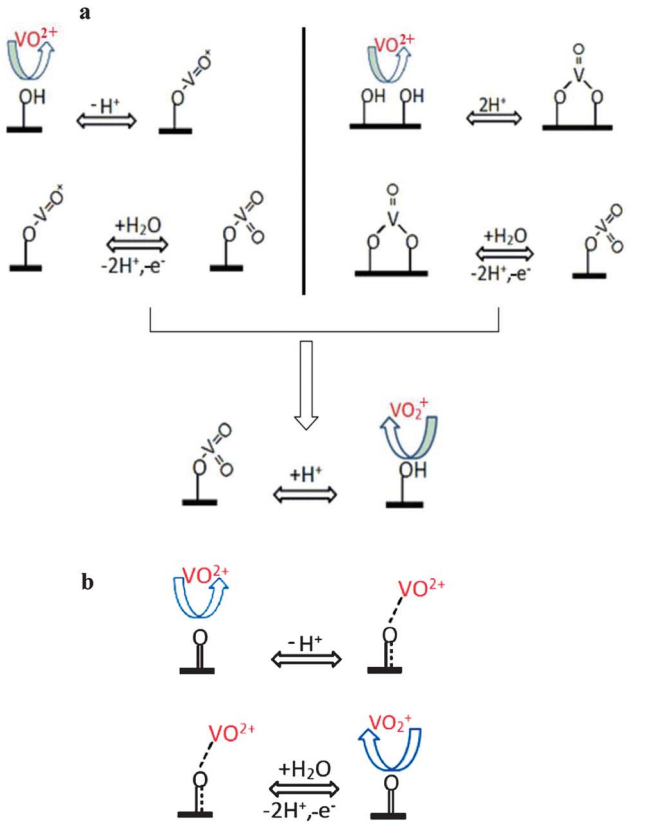

Scheme 1 The redox reaction of VO^{2+}/VO_2^+ during charging–discharging *via* catalytic activity with hydroxyl (–OH) (scheme a) and carbonyl (C=O) (scheme b) functional groups.

electrolyte. This enhanced specific capacitance further confirms the occurrence of redox reaction of VO^{2+}/VO_2^+ at electrode–electrolyte interface. Moreover, this is higher than the specific capacitance of composite electrodes using symmetric supercapacitors for example PANI/GO (555 F g^{-1})[27b] as well as some redox additive electrolyte using EDLCs such as *m*-methylene blue (279 F g^{-1}),[9] lignosulfonates (178 F g^{-1}),[10] *m*-phenylenediamine (78 F g^{-1})[14] and *p*-phenylenediamine (605.33 F g^{-1}).[12]

Fig. 5e shows that the specific capacitance decreases with increasing current density. However, relatively 66.2% of capacitance (417.5 F g^{-1}) retention was found for $VOSO_4$ added 1 M H_2SO_4 electrolyte at higher current density (20 mA cm^{-2}) while it was about 47.5% (209.2 F g^{-1}) for pristine 1 M H_2SO_4. Besides, the $VOSO_4$ added 1 M H_2SO_4 electrolyte shows the low coulombic efficiency (77.3%) compared to pristine electrolyte (80.9%) at 1 mA cm^{-2} whereas this result could be associated with kinetics of VO^{2+}/VO_2^+ redox reaction. However, both electrolytes show the maximum coulombic efficiency of ~98% at higher current density (97.8% for $VOSO_4$ added 1 M H_2SO_4 electrolyte and 98.4% for pristine electrolyte at 20 mA cm^{-1}). Interestingly, the IR drop decreased from 0.022 V to 0.01 V (Fig. 5d) due to the effect of $VOSO_4$ in 1 M H_2SO_4. This decreasing IR drop value can also improve the performance of the EDLC, based on the relation[28,29a] $E = 0.5C\,[(V_{initial} - IR)^2 - V_{final}^2]$. If IR drop is high, energy loss is unavoidable. The equivalent series resistance (ESR) of the EDLCs are also calculated[14] (ESR = $IR_{drop}/2I$, where I is current density) from charge–discharge curve and obtained the lower ESR value of 5 Ω over pristine 1 M H_2SO_4 (11 Ω) and it indicates the improved ionic conductivity in electrolyte.

Nevertheless, a higher energy density of 13.7 W h kg^{-1} was obtained than with pristine electrolyte (9.3 W h kg^{-1}) at 1 mA cm^{-2}. It is nearly 47% of energy density increment than pristine (Fig. 5f). This obtained energy density is even comparable and higher than that of previous redox-active electrolyte using EDLCs such as indigo carmine (1.7 W h kg^{-1}),[2] *m*-phenylenediamine (9.99 W h kg^{-1})[14] and *p*-phenylenediamine (4.23 W h kg^{-1}).[13] As well as higher than the reported asymmetric supercapacitors such as TiP_2O_7//AC (13 W h kg^{-1}),[29b] TiO_2 (B)//CNT (12.5 W h kg^{-1})[29c] PEDOT//MnO_2 (13.5 W h kg^{-1}),[32] AC//MnO_2 (10.4 W h kg^{-1}),[33] CNT//graphene/MnO_2 (12.5 W h kg^{-1}),[34] AC//RuO_2/TiO_2 (5.7 W h kg^{-1}),[35] MnO_2//Fe_3O_4 (8.1 W h kg^{-1})[36] and PPy/PMA//PEDOT/PTA (4 W h kg^{-1}).[37] Unfortunately, there is no significant increment in power density after introducing $VOSO_4$ *i.e.*, 315.2 W Kg^{-1} for 1 M H_2SO_4 electrolyte and 325 W Kg^{-1} for $VOSO_4$ + 1 M H_2SO_4 electrolyte. This may due to the decreasing IR drop or ESR after addition of $VOSO_4$.

The Nyquist impedance and admittance spectra of EDLCs are shown in Fig. 6a and Fig. S4a†, respectively. The solution resistance (R_s) and charge transfer resistance (R_{ct}) of EDLCs was calculated by fitting of EIS using equivalent circuit and is shown in inset of Fig. 6a, which includes a solution resistance (R_s), charge transfer resistance (R_{ct}), electrical double layer element (C_{edl}), pseudocapacitance element (C_{pse}) and Warburg impedance (W). Here, electrical double layer element (C_{edl}), pseudocapacitance element (C_{pse}) indicates the presence of capacitance and pseudocapacitance through adsorption of electrolyte's ions and electron-transfer or redox reaction of electrolyte's ions. The calculated solution resistance of 1 M H_2SO_4 and 0.3 g $VOSO_4$ + 1 M H_2SO_4 electrolytes are 1.5 Ω and 0.8 Ω whereas the measured charge transfer resistance in the electrodes are 3 Ω and 1.6 Ω respectively. However, the addition of $VOSO_4$ in 1 M H_2SO_4 reduces the charge transfer resistance and reveals the improved ionic conductivity at electrode–electrolyte interface. Moreover, the small diameter semicircle is noted for $VOSO_4$ + 1 M H_2SO_4 electrolyte which characterizes its lower ionic resistance.[30] Similarly, the knee frequency also increased (Fig. S4a†) from 25.36 Hz to 53.98 Hz for the $VOSO_4$

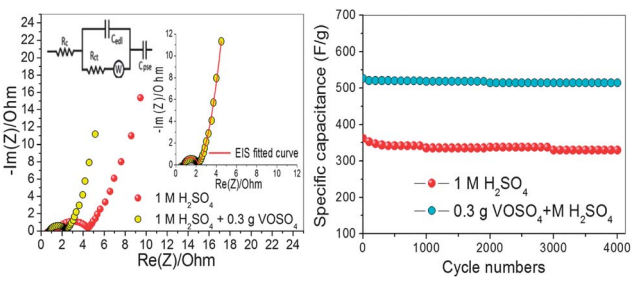

Fig. 6 (a) Nyquist plots (inset: equivalent circuit and fitted EIS curve); (b) variation of specific capacitance with respect to cycles at 5 mA cm^{-2} of 1 M H_2SO_4 and $VOSO_4$ + 1 M H_2SO_4 electrolyte.

added electrolyte which also denoted the improved performance.[31] Fig. S4b† shows the real part capacitance (C') as a function of frequency of EDLCs. As well, it describes the increased capacitance after adding $VOSO_4$ in 1 M H_2SO_4 electrolyte at low frequency which is consistent with the results of CV and GCD. The variation of specific capacitance with cycle numbers at 5 mA cm^{-2} is shown in Fig. 6b. The specific capacitance of $VOSO_4$ + 1 M H_2SO_4 electrolyte decreases from 527 to 514.2 F g^{-1} with better capacitance retention of 97.57% than 1 M H_2SO_4 electrolyte (91%) after 4000 cycles.

It is well known that liquid electrolytes have issues in packing, leakage, corrosion and so on. In this regard, currently the gel electrolytes are more interesting for EDLCs applications. Here, $VOSO_4$ + 1 M H_2SO_4 electrolyte was used to prepare the gel electrolyte. Subsequently, the EDLC was fabricated using $VOSO_4$ + 1 M H_2SO_4 added gel polymer electrolyte (for details see ESI†). Fig. 7a–d shows the CV at 5–200 mV s^{-1}, GCD at 1–20 mA cm^{-2}, specific capacitance as function of current density and output performance of the polymer gel electrolyte used in the EDLC. The CV retains its shape even at high scan rate of 200 mV s^{-1}, which reveals a better electrochemical retention property. From GCD, the maximum specific capacitance of 585 F g^{-1} with energy density of 12.83 W h kg^{-1} is achieved at 1 mA cm^{-2}. Here the decreased specific capacitance or energy density may be due to the lack of better contact between the porous electrode surface and polymer electrolyte. However, it is a very common problem for polymer electrolyte used in EDLCs and also these obtained values are comparable with the liquid electrolyte. In addition, this EDLC exhibits the coulombic efficiency of 63.8% and 97% at 1 mA cm^{-2} and 20 mA cm^{-2} (Fig. 7c), respectively. The charged EDLC (Fig. 7d) at 1 mA cm^{-2} delivered the output voltage of 0.68 V (see video, ESI†). So this approach opens up a new avenue for the possible application especially for portable electronics.

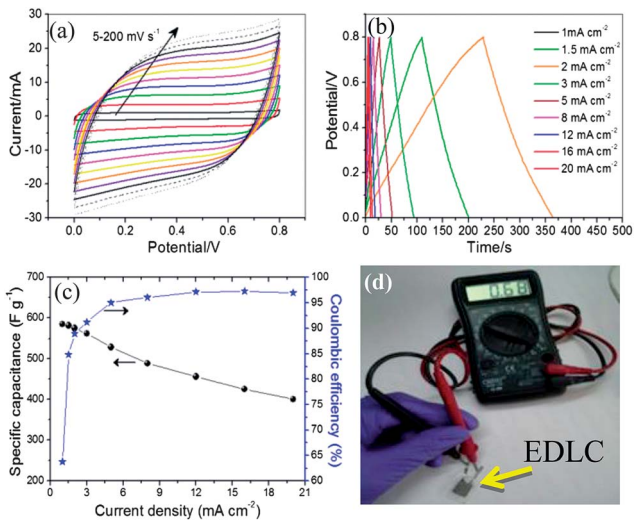

Fig. 7 Electrochemical characteristics of gel polymer electrolyte used in EDLC: (a) CV curves at 5–200 mV s^{-1}; (b) charge–discharge discharge curves at 1–20 mA cm^{-2}; (c) specific capacitance and coulombic efficiency as function of current density; (d) performance of polymer electrolyte used EDLC.

4 Conclusions

Porous activated carbon was prepared from *Eichhornia crassipes* by NaOH activation. The EDLC using $VOSO_4$ added 1 M H_2SO_4 electrolyte showed maximum specific capacitance of 630.6 F g^{-1} at 1 mA cm^{-2} which is ~43% of improved specific capacitance than 1 M H_2SO_4 (440.6 F g^{-1}). Subsequently, the energy density also increased from 9.3 to 13.7 W h kg^{-1} at 1 mA cm^{-2}. The IR drop or ESR value also decreased after adding $VOSO_4$ in 1 M H_2SO_4. From the above results it is confirmed that the redox pair VO^{2+}/VO_2^{+} can enhance the overall electrochemical properties of EDLC. These results could establish that $VOSO_4$ added 1 M H_2SO_4 is an excellent candidate to improve the performance of the EDLCs.

Acknowledgement

The authors are grateful to the Department of Atomic Energy-Board of Research in Nuclear Sciences (DAE–BRNS), Government of India (no. 2010/37P/46/BRNS/1443) for their financial support.

Notes and references

1 S. Roldan, C. Blanco, M. Granda, R. Menendez and R. Santamaria, *Angew. Chem., Int. Ed.*, 2011, **50**, 1699–1701.
2 S. Roldan, C. Blanco, M. Granda, R. Menendez and R. Santamaria, *Electrochim. Acta*, 2011, **56**, 3401–3405.
3 K. Fic, G. Lota, M. Meller and E. Frackowiak, *Energy Environ. Sci.*, 2012, **5**, 5842–5850.
4 L. Zhao, L. Z. Fan, M. Q. Zhou, H. Guan, S. Qiao, M. Antonietti and M. M. Titirici, *Adv. Mater.*, 2010, **22**, 5202–5206.
5 D. H. Jurcakova, A. M. Puziy, O. I. Poddubnaya, F. S. Garcia, J. M. D. Tascon and G. Q. Lu, *J. Am. Chem. Soc.*, 2009, **131**, 5026–5027.
6 D. W. Wang, Z. G. Chen, G. Q. Li and H. M. Cheng, *Chem. Mater.*, 2008, **20**, 7195–7200.
7 (*a*) C. G. Liu, Y. S. Lee, Y. J. Kim, I. C. Song and J. H. Kim, *Synth. Met.*, 2009, **159**, 2009; (*b*) K. Karthikeyan, S. Amaresh, V. Aravindan and Y. S. Lee, *J. Mater. Chem. A*, 2013, **1**, 4105–4111; (*c*) M. T. Lee, C. Y. Fan, Y. C. Wang, H. Y. Li, J. K. Chang and C. M. Tseng, *J. Mater. Chem. A*, 2013, **1**, 3395–3405.
8 (*a*) K. Zhang, L. L. Zhang, X. S. Zhao and J. Wu, *Chem. Mater.*, 2010, **22**, 1392–1401; (*b*) Z. Lei, Z. Chen and X. S. Zhao, *J. Phys. Chem. C*, 2010, **114**, 19867–19874; (*c*) R. B. Rakhi, W. Chen and H. N. Alshareef, *J. Mater. Chem.*, 2012, **22**, 5177–5183; (*d*) L. L. Zhang, S. Zhao, X. N. Tian and X. S. Zhao, *Langmuir*, 2010, **26**, 17624–17628.
9 S. Roldan, M. Granda, R. Menendez, R. Santamaria and C. Blanco, *Electrochim. Acta*, 2012, **83**, 241–246.
10 G. Lota and G. Milczarek, *Electrochem. Commun.*, 2011, **13**, 470–473.
11 J. Hu, H. Yu, L. Fan, G. Luo, J. Lin and M. Huang, *J. Mater. Chem.*, 2012, **22**, 19025–19030.

12 H. Yu, J. Wu, J. Lin, L. Fan, M. Huang, Y. Lin, Y. Li, F. Yu and Z. Qiu, *ChemPhysChem*, 2013, **14**, 394–399.
13 H. Yu, L. Fan, J. Wu, Y. Lin, M. Huang, J. Lin and Z. Lan, *RSC Adv.*, 2012, **2**, 6736–6740.
14 (*a*) W. Li, J. Liu and C. Yan, *Carbon*, 2011, **49**, 3463–3470; (*b*) C. Flox, J. R. Garcia, R. Nafria, R. Zamani, M. Skoumal, T. Andreu, J. Arbiol, A. Cabot and J. R. Morante, *Carbon*, 2012, **50**, 2372–2374; (*c*) W. Li, J. Liu and C. Yan, *Carbon*, 2013, **55**, 313–320.
15 S. T. S. Kumar, R. K. Selvan, N. Ponpandian and J. S. Melo, *RSC Adv.*, 2012, **2**, 8937–8940.
16 (*a*) K. C. Ng, S. Zhang, C. Peng and G. Z. Chen, *J. Electrochem. Soc.*, 2009, **156**, A846–A853; (*b*) Z. Niu, W. Zhou, J. Chen, G. Feng, H. Li, W. Ma, J. Li, H. Dong, Y. Ren, D. Zhao and S. Xie, *Energy Environ. Sci.*, 2011, **4**, 1440–1446.
17 (*a*) J. Zhang, J. Jiang, H. Li and X. S. Zhao, *Energy Environ. Sci.*, 2011, **4**, 4009–4015; (*b*) W. Chen, R. B. Rakhi, L. Hu, X. Xie, Y. Cui and H. N. Alshareef, *Nano Lett.*, 2011, **11**, 5165; (*c*) K. P. S. Prasad, D. S. Dhawale, T. Sivakumar, S. S. Aldeyab, J. S. M. Zaidi, K. Ariga and A. Vinu, *Sci. Technol. Adv. Mater.*, 2011, **12**, 044602–044609.
18 S. T. S. Kumar, R. K. Selvan, Y. S. Lee and J. S. Melo, *J. Mater. Chem. A*, 2013, **1**, 1086–1095.
19 W. Huang, H. Zhang, Y. Huang, W. Wang and S. Wei, *Carbon*, 2011, **49**, 838–843.
20 W. Xing, C. C. Huang, S. P. Zhuo, X. Yuan, G. Q. Wang, D. H. Jurcakova, Z. F. Yan and G. Q. Lu, *Carbon*, 2009, **47**, 1715–1722.
21 S. T. S. Kumar, B. S. Kumar, S. Balaji, C. Sanjeeviraja and R. K. Selvan, *Mater. Res. Bull.*, 2011, **46**, 413–419.
22 M. Sevilla and A. B. Fuertes, *Carbon*, 2009, **47**, 2281–2289.
23 M. Li, W. Li and S. Liu, *Carbohydr. Res.*, 2011, **346**, 999–1004.
24 E. Frackowiak, *J. Braz. Chem. Soc.*, 2006, **6**, 1074–1082.
25 D. S. Su and R. Schogl, *ChemSusChem*, 2010, **3**, 136–168.
26 W. Li, J. Liu and C. Yan, *Carbon*, 2011, **49**, 3463–3470.
27 (*a*) W. Li, J. Liu and C. Yan, *Carbon*, 2013, **55**, 313; (*b*) J. J. Xu, K. Wang, S. Z. Zu, B. H. Han and Z. X. Wei, *ACS Nano*, 2010, **4**, 5019–5026.
28 Z. Chen, V. Augustyn, X. Jia, Q. Xiao, B. Dunn and Y. Lu, *ACS Nano*, 2012, **5**, 4319–4328.
29 (*a*) B. Fang and L. Binder, *J. Phys. Chem. B*, 2006, **110**, 7877–7882; (*b*) V. Aravindan, M. V. Reddy, S. Madhavi, S. G. Mhaisalkar, G. V. S. Rao and B. V. R. Chowdari, *J. Power Sources*, 2011, **196**, 8850–8854; (*c*) Q. Wang, Z. Wen and J. Li, *Adv. Funct. Mater.*, 2006, **16**, 2141–2146.
30 X. He, L. Jiang, S. Yan, J. Lei, M. Zheng and H. Shui, *Diamond Relat. Mater.*, 2008, **17**, 993–998.
31 W. Wei, X. Cui, W. Chen and D. G. Ivey, *J. Power Sources*, 2009, **186**, 543–550.
32 V. Khomenko, E. Raymundo-Pinero, E. Frackowiak and F. Benguin, *Appl. Phys. A: Mater. Sci. Process.*, 2006, **82**, 599–606.
33 Y. T. Wang, A. H. Lu, H. L. Zhang and W. C. Li, *J. Phys. Chem. C*, 2011, **115**, 5413–5421.
34 G. H. Yu, L. B. Hu, M. Vosgueritchian, H. L. Wang, X. Xie, J. R. McDonough, X. Cui, Y. Cui and Z. N. Bao, *Nano Lett.*, 2011, **11**, 2905–2911.
35 Y. G. Wang, Z. D. Wang and Y. Y. Xia, *Electrochim. Acta*, 2005, **50**, 5641–5646.
36 C. Liu, Z. Yu, D. Neff, A. Zhamu and B. Z. Jang, *Nano Lett.*, 2010, **10**, 4863–4868.
37 G. M. Suppes, C. G. Cameron and M. S. Greund, *J. Electrochem. Soc.*, 2010, **157**, A1030–A1034.